



From hydrated silica to quartz: Potential hydrothermal precipitates found in Jezero crater, Mars

P. Beck^{a,*}, O. Beyssac^b, E. Dehouck^c, S. Bernard^b, M. Pineau^{c,d}, L. Mandon^a, C. Royer^e, E. Clavé^f, S. Schröder^f, O. Forni^g, R. Francis^h, N. Mangoldⁱ, C.C. Bedford^j, A.P. Broz^k, E.A. Cloutis^l, J.R. Johnson^m, F. Pouletⁿ, T. Fouchet^o, C. Quantin-Nataf^c, C. Pilorget^{n,p}, W. Rapin^g, P.-Y. Meslin^g, T.S.J. Gabriel^q, G. Arana^r, J.M. Madariaga^r, A.J. Brown^s, S. Maurice^g, S.M. Clegg^t, O. Gasnault^g, A. Cousin^g, R.C. Wiens^j, the SuperCam team

^a Univ. Grenoble Alpes, CNRS, IPAG, 38000 Grenoble, France

^b Sorbonne Université, Muséum National d'Histoire Naturelle, UMR CNRS 7590, Institut de Minéralogie, de Physique des Matériaux et de Cosmochimie, IMPMC, 75005 Paris, France

^c Université de Lyon, UCBL, ENSL, CNRS, LGL-TPE, Lyon, France

^d Laboratoire d'Astrophysique de Marseille (LAM), Marseille, France

^e LATMOS, CNRS, Univ. Saint-Quentin-en-Yvelines, Sorbonne Univ, France

^f Deutsches Zentrum für Luft- und Raumfahrt (DLR), Institute of Optical Sensor Systems, 12489 Berlin, Germany IRAP, Toulouse, Germany

^g IRAP, CNRS, Université de Toulouse, UPS-OMP, Toulouse, France

^h Jet Propulsion Laboratory, California Institute of Technology, USA

ⁱ Laboratoire Planétologie et Géosciences, CNRS, Université Nantes, Université Angers, UMR 6112, 44322 Nantes, France

^j Purdue University Earth, Atmospheric and Planetary Sciences department, West Lafayette, IN, USA

^k University of Oregon, USA

^l Department of Geography, University of Winnipeg, 515 Portage Avenue, Winnipeg, Manitoba, R3B 2E9, Canada

^m John Hopkins University Applied Physics Laboratory, Laurel, MD, USA

ⁿ Institut d'Astrophysique Spatiale (IAS), CNRS/Paris-Saclay University, France

^o LESIA, Observatoire de Paris, Université PSL, CNRS, Sorbonne Université, Université Paris Cité, 5 place Jules Janssen, 92195 Meudon, France

^p Institut Universitaire de France

^q U.S. Geological Survey, Flagstaff, AZ, USA

^r Univ. Basque Country (UPV/EHU)

^s Planicius Research, USA

^t Los Alamos National Laboratory, Los Alamos, NM, USA

ARTICLE INFO

Keywords:

Mars
M2020
Opal
Hydrated silica
Biosignature
Quartz

ABSTRACT

On Earth, silica-rich phases from opal to quartz are important indicators and tracers of geological processes. Hydrated silica, such as opal, is a particularly good matrix for the preservation of molecular and macroscopic biosignatures. Cherts, a type of silica-dominated rocks, provide a unique archive of ancient terrestrial life while quartz is the emblematic mineral of the Earth's continental crust. On Mars, hydrated silica has been detected in several locations based on remote sensing and rover-based studies. In the present article we report on the detection of cobbles made of hydrated silica (opal or chalcedony), as well as well-crystallized quartz. These detections were made with the SuperCam instrument onboard Perseverance (Mars 2020 mission), using a combination of LIBS, infrared and Raman spectroscopy. Quartz-dominated stones are detected unambiguously for the first time on the Martian surface, and based on grain size and crystallinity are proposed to be of hydrothermal origin. Although these rocks were all found as float, we propose that these detections are part of a common hydrothermal system, and represent different depths / temperatures of precipitation. This attests that hydrothermal processes were active in and around Jezero crater, possibly triggered by the Jezero crater-forming impact. These silica-rich rocks, in particular opaline silica, are very promising targets for sampling and return to Earth given their high biosignature preservation potential.

* Corresponding author.

E-mail address: pierre.beck@univ-grenoble-alpes.fr (P. Beck).

<https://doi.org/10.1016/j.epsl.2025.119256>

Received 4 September 2024; Received in revised form 9 February 2025; Accepted 10 February 2025

Available online 28 February 2025

0012-821X/© 2025 The Authors. Published by Elsevier B.V. This is an open access article under the CC BY license (<http://creativecommons.org/licenses/by/4.0/>).

1. Introduction

NASA's Mars 2020 *Perseverance* rover is exploring Jezero crater on Mars since February 2021, with the aim to collect a set of samples to be returned to Earth in a later mission, where they will be scrutinized to identify organic traces of ancient life, as part of the Mars 2020 mission and the Mars Sample Return Program (e.g., Farley et al., 2020). One of the four major science goals of the mission is also to assess the bio-signature preservation potential of the site (Farley et al., 2020). To this end, rocks containing hydrated silica and other silica-rich phases currently represent the most promising astropaleontological targets (McMahon et al., 2018). On Earth, some of the oldest organic microfossils reported so far have been found in cherts, i.e. silica-rich rocks (Walsh and Lowe, 1985; Alleon et al., 2016a, 2018). Cherts are thus now recognized as exceptional windows for the morphological preservation of organic microfossils (i.e. "Bitter Springs-type preservation" - Butterfield, 2003), as are opals (e.g., Chauviré et al., 2020). One explanation lies in the protective role of hydrated silica matrices because early entombment within silica minimizes the molecular degradation of microorganisms during subsequent diagenesis (Oehler, 1976; Alleon et al., 2016b).

Hydrated silica generally forms from prolonged exposure of silicate rocks to abundant water. Hydrated silica consists of a mixture of silica (SiO₂) and "water", in the form of both -OH groups and H₂O molecules (Jones & Segnit, 1971), and can exhibit a diversity of crystallinity, shapes, mesoscopic arrangements of the silica domains, and/or amounts of OH/H₂O. This diversity is a result of the variety of protoliths, geological contexts, and alteration pathways from which it can form (Rice et al., 2013; Chauviré et al., 2017). Opals, the less crystalline forms of hydrated silica, can be identified and classified based on their X-ray diffraction patterns. On Earth, opals are generally less than a few Ma old (Rice et al., 2013) since they inevitably transform to more "crystalline" forms upon burial-heating and interaction with H₂O, eventually forming chalcedony (made of fibrous and cryptocrystalline quartz), or cherts (made of massive deposits of cryptocrystalline quartz). At higher temperatures, quartz may form by saturation in SiO₂ of a fluid during hydrothermal processes.

On Mars, variably-hydrated silica has been identified in various places across the surface, based on orbital near-infrared (NIR: 0.7–1 μm) and short-wave infrared (SWIR: 1–2.5 μm) reflectance spectra (Milliken et al., 2008; Skok et al., 2010; Pan and Ehlmann, 2014; Sun and Milliken, 2018; Tarnas et al., 2019; Pineau et al., 2020; Liu et al., 2022), thermal infrared emissivity spectra, and in situ rover observations at Gusev and Gale craters (Bandfield, 2008; Squyres et al., 2008; Ruff et al., 2011; Bandfield et al., 2013; Smith et al., 2013; Morris et al., 2016). Hydrated silica seems to be particularly present in sedimentary fan deposits (Pan et al., 2021) and was consistently detected from orbit in Jezero crater (Tarnas et al., 2019; Carter et al., 2023). Quartz, which is usually anhydrous, cannot be directly detected from orbit in the NIR or SWIR since it does not have a diagnostic signature in this spectral range. The only prior report of quartz occurrence at the surface of Mars is from X-ray diffraction by the CheMin instrument onboard the MSL rover as a minor phase in the sands of Gale crater, with abundances <1.5 wt.% total phases, close to the detection limit (Rampe et al., 2018).

Here, we report on the detection of silica-dominated targets in Jezero crater from three different locations. Three distinct types of silica material were found in three distinct locations; opaline silica, chalcedony, and finally quartz, which is detected as the dominant phase unambiguously for the first time on the surface of Mars.

2. Previous in situ detection of hydrated silica and quartz from Mars

Before SuperCam's detection, hydrated silica-rich deposits had been detected in situ by rovers in three distinct locations. One was detected at Home Plate in Gusev crater by *Spirit* (Squyres et al., 2008) using a

combination of elemental composition from the Alpha Particle X-ray Spectrometer (APXS), iron mineralogy from the Mössbauer spectrometer, and silicate mineralogy from Mini-TES mid-infrared spectroscopy. The hydrated silica was found to be opaline based on the intensity and position of the SiO₄ bending and stretching modes, and its mode of occurrence was interpreted as a hydrothermal sinter deposit (Ruff et al., 2011). In some cases, the presence of a 1625 cm⁻¹ emissivity maximum was reported and attributed to the bending mode of H₂O, which would produce absorption at 1.4 and 1.9 μm in the SWIR. This deposit is located a few hundred meters away from the Comanche outcrop where Fe/Mg-carbonates were identified (Morris et al., 2010), in a mixture with olivine and amorphous silicate. However, the geochemical and stratigraphic connections between these two units are not clearly understood.

Hydrated silica was also observed in Gale crater by the *Curiosity* rover. It was suggested as a component of the amorphous material observed in X-ray diffraction patterns measured by CheMin (Smith et al., 2021). It was particularly abundant in a mudstone from the Maria's Pass location, in the Murray Formation (Morris et al., 2016). The presence of hydrated silica was also confirmed by ChemCam at this location (Rapin et al., 2018; Gabriel et al., 2022) based on the MOC chemistry and analysis of the hydrogen signal. Hydrated silica also occurs in light-toned, fracture-associated halos within sandstones overlying the Murray formation mudstones (Frydenvang et al., 2017; Yen et al., 2017). The suspected type of hydrated silica is Opal-A (Rapin et al., 2018), with formation through acid-leaching and/or passive silica enrichment by aqueous fluids. The occurrence of the hydrated silica (veins and halos) and the nature of the protolith are distinct between observations in Gale and Gusev craters.

More recently, the *Zhurong* rover that landed in Utopia Planitia detected hydrated silica using its MarsCoDe SWIR spectrometer (Liu et al., 2022). This detection arose from the observation of a 2.2-μm band whose position and shape seem more like Si-OH than Al-OH. This band was also associated with a 1.4-μm and a 1.9-μm band. The latter has maxima around 1.94–1.95 μm, which led Liu et al. (2022) to suspect that hydrated sulfates could be present together with hydrated silica. The formation scenario preferred by the authors is the dissolution and reprecipitation of silica by upwelling H₂O from an underlying water table, leading to the formation of a duricrust (a silcrete if dominated by hydrated silica).

Crystalline silica phases (quartz and other SiO₂ polymorphs) lack diagnostic absorption bands in the visible and NIR domain. They have been inferred in some specific evolved lithologies based on mid-IR spectroscopy (Bandfield et al., 2004) but not detected directly from orbit (see Malarewicz et al., in press and reference therein). At Gale crater, MSL *Curiosity* reported in situ the occurrence of tridymite in high-SiO₂ sedimentary rock (Morris et al., 2016) and traces of quartz in the sands of the Bagnold dune (Rampe et al., 2018) based on X-ray diffraction data with the CheMin instrument. Silica crystalline phases are reported as well in a few Martian meteorites. Quartz with minor cristobalite is observed in small late-stage and interstitial crystallization pockets in meteorites (Filiberto et al., 2018). Quartz has also been reported with K-feldspar and plagioclase and other mineral phases forming pre-Noachian granitic clasts in the Martian regolith breccia NWA 7533 (Malarewicz et al., in press).

3. Methods

Since its landing in 2021, the *Perseverance* rover has been investigating and sampling rocks from Jezero crater. This mission began with the characterization of the igneous rocks from the crater floor, followed by an ascent onto sediments from the Jezero western Delta-Fan. It then began exploring the Margin Unit, an enigmatic deposit where signatures of olivine and carbonates were detected from orbit (Carter et al. 2023; Horgan et al. 2020). Then, it began climbing the western part of the crater rim.

Silica-dominated targets were identified using the combination of VISIR (visible/near infrared), Raman spectroscopy, and LIBS (Laser-Induced Breakdown Spectroscopy). Some of the targets discussed here were selected tactically by the Mars 2020 team according to Mars 2020 mission priorities (e.g. Farley et al., 2020), while two of them were selected by the AEGIS algorithm (Autonomous Exploration for Gathering Increased Science; Francis et al., 2017). The AEGIS algorithm is an onboard automatic targeting method that has been implemented in SuperCam modes of operations (Wiens et al., 2021; Maurice et al., 2021). The RMI (Remote Micro Imager) mosaic of the targets are shown (Fig. 1), and VISIR spectra were obtained on several locations of the targets (Fig. 1). Typically, at a ~3 m distance to the target, the fields of views are 2.2 mm and 3.5 mm in diameter for visible (VIS) and near-infrared (IR) spectra, respectively, while the area analyzed by LIBS varies from about 0.16 mm at 2 m up to 0.45 mm at 7 m (Maurice et al., 2021).

SuperCam provides information on the chemistry of rocks within about 10 m of the rover using LIBS. The plasma emission generated by focusing a pulsed laser onto the target is analyzed by multiple spectrometers and emission lines can be used to derive the elemental composition for each point (Anderson et al., 2022). The algorithm used is the one presented in Anderson et al. (2022), which provides

major-element oxide compositions (MOC) in weight % (wt. %). The typical root mean square error of prediction (RMSEP) accuracies in wt. %, are: CaO (1.3), FeO (3.1), Na₂O (0.5), K₂O (0.6), MgO (1.1), SiO₂ (6.1), TiO₂ (0.3) (Anderson et al. 2022).

In addition to major elements, several key light elements can be detected through LIBS, in particular hydrogen and sulfur. The hydrogen signal was analyzed using spectral unmixing scores (Schröder et al., 2023). The sulfur signal was investigated by comparing the spectra of the targets to those of the sulfur-rich calibration target (Cousin et al., 2022) and a S-rich vein analyzed in situ by SuperCam. The carbon signal is more challenging to interpret due to atmospheric contributions. Still carbon-rich points (>4.5 wt.% C) can be identified with LIBS on Mars (Clavé et al., 2023) but they were not detected in the targets discussed here.

The SuperCam InfraRed Spectrometer (IRS) measures reflected sunlight in the 1.3–2.6 μm range (Fouchet et al., 2022), with a spectral resolution ranging from 5 (at 1.3 μm) to 20 nm (at 2.6 μm). Reflectance spectra from the targets were calibrated using the procedures described in Royer et al. (2023). SuperCam visible (VIS) spectra were also collected (0.40–0.85 μm), but are not used here.

SuperCam Raman is a remote technique using a telescope to collect the Raman signal generated by a pulsed laser (532 nm) collimated on the

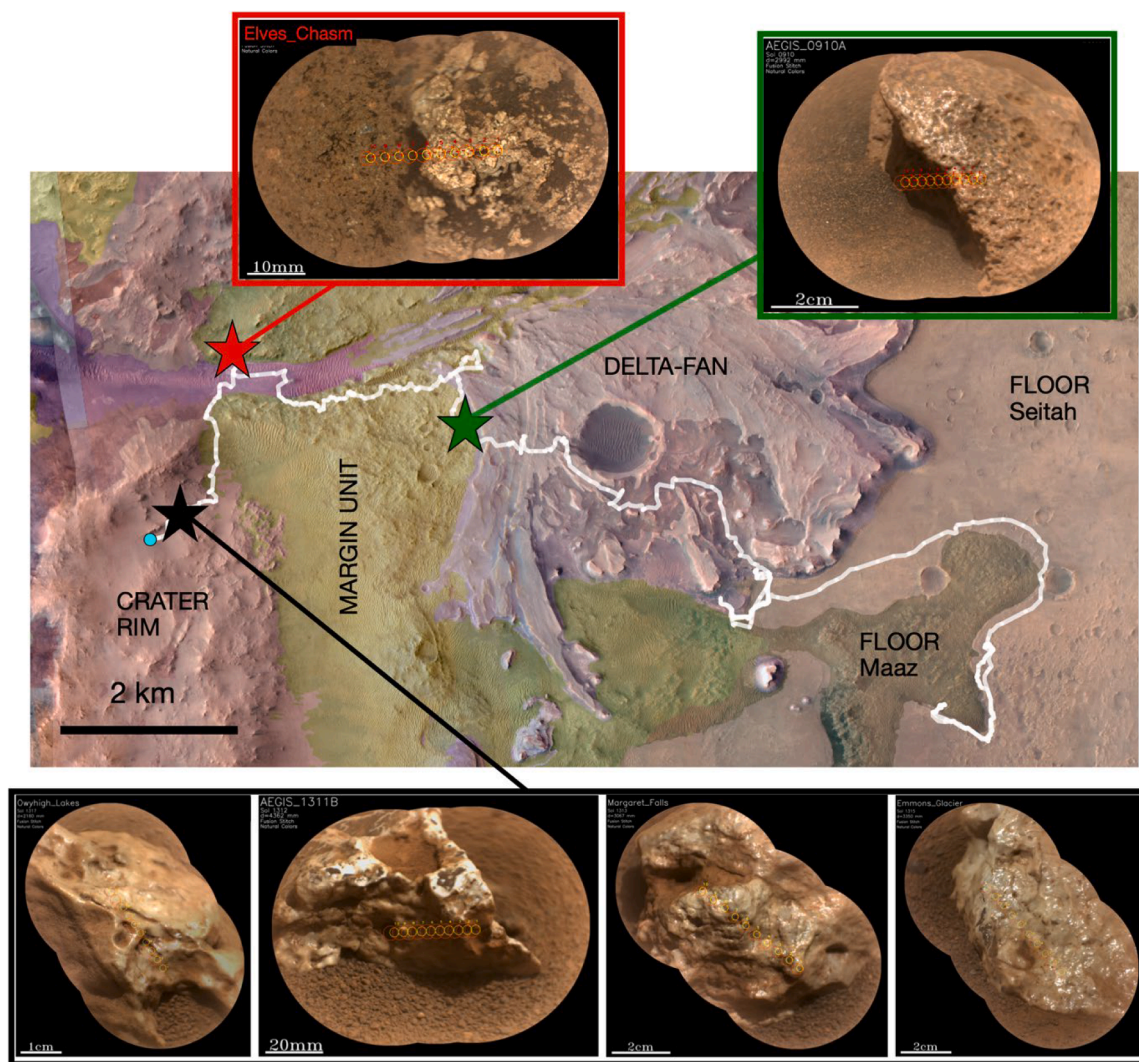


Fig. 1. Annotated geologic map of units within Jezero crater, superimposed on color imaging, with the location of the high-silica targets indicated by red (opal), green (chalcedony) and black (quartz) stars. The white line is the location of the rover traverse and rover stops since landing. For each of the three locations, RMI images of high-silica targets are also shown. On these RMI images, the red circles correspond to the field of view of SuperCam infrared reflectance spectra, while the yellow circles correspond to the field of view of the visible part of the reflectance spectra.

surface of the target. The analytical footprint varies with the distance to the target (field of view = 0.75 mrad) from 1.5 mm in diameter at 2 m up to 3 mm at 4 m. This analytical footprint is much larger compared to the micrometric spot size used by most laboratory spectrometers. SuperCam Raman uses time-resolved spectroscopy to reject the daylight entering the telescope, and to reject the luminescence signal which may be present for many minerals. SuperCam Raman spectra are obtained routinely by averaging the signal from 400 laser shots for each analyzed point. More details on SuperCam Raman may be found in Clavé et al. (2024b). For comparison with Martian data, we performed some additional analyses in the laboratory on three reference samples: a chert from Lake Magadi with quartz grain size <2 µm, a sandstone from Fontainebleau (France) with anisotropic quartz grain size in the range 20 to 270 µm, and on a centimeter-size crystal of hydrothermal quartz from Minas Gerais (Brazil). The instrument used in the laboratory is a testbed for SuperCam Raman using a similar configuration and is described by Fau et al. (2019) and Clavé et al. (2024b).

4. Observations

4.1. Context and texture of the rock

Perseverance landed on the floor of Jezero crater where it characterized two geological units of igneous origin: the basaltic lava flows of the Mááz unit (Udry et al., 2023) and the underlying olivine-rich cumulate rocks of the Séitah unit (Beyssac et al., 2023). Then, the rover explored the sedimentary rocks of the Jezero western fan which are dominated by olivine-rich sandstones. No silica-rich target was observed in either the Crater Floor Unit, nor in the delta. Then the rover entered the Margin Unit of enigmatic origin but composed of olivine-rich rocks of ultramafic composition showing various degrees of alteration as attested by the pervasive presence of Fe-Mg carbonates and a minor silica phase (Clavé et al., 2024a). Finally, the rover climbed to the Crater Rim Unit at the edge of the crater. All silica-rich targets analyzed here were found as float rocks in the Margin Unit and the crater rim, yet we cannot say with certainty that they originate from these units or elsewhere in the Jezero area.

The first detection of high-silica material occurred on sol 910 and was selected using AEGIS software shortly after *Perseverance* entered the Margin Unit of Jezero crater (Horgan et al., 2020). The target (*AEGIS_910A*; see Fig. SOM1) is a light-toned, partially buried float rock with a shiny luster and is roughly 5 cm in diameter. It displays a pitted texture (typical pit size 1–2 mm), and the surface is partially covered by sand or dark-toned dust coatings. Some of the VISIR analyses are shadowed but spectra with good signal-to-noise ratio were obtained on locations 1 to 4 (Fig. 1).

The second observation (target *Elves_Chasm*; all SuperCam data is available publicly and permanently at <https://pds-geoscience.wustl.edu>) was also made close to the edge of the Margin Unit, but in that case in the northern-most part of the unit (Fig. 1). Silica-rich material was found as bright clast/inclusion embedded in darker olivine- and clay-rich material. In this target 5 LIBS and 5 VISIR points cover well the bright clast/inclusion and reveal very specific chemistry and mineralogy. This bright material has a granular “pop-corn” appearance (Fig. 1).

The third set of silica-rich material was found during the Crater Rim campaign, when the rover was climbing through a suite of rocks of ultramafic to felsic chemistry. Si-rich material corresponds to light-gray float rocks, with a vitreous luster. Four targets (*Emmons_Glacier*, *AEGIS_1331B*, *Margaret_Falls* and *Owyhigh_Lakes*) were analyzed by the SuperCam instrument and we find them to be silica-dominated.

4.2. LIBS-derived elemental chemistry

The LIBS derived elemental chemistry revealed strong enrichment in Si for all 6 targets. These rocks clearly stand out among the >9000

individual chemical analysis performed by SuperCam since the beginning of the mission (Fig. 2).

Inspection of the individual lines in the LIBS spectra, dominated by Si- and O-lines (Fig. SOM2) suggests that the *AEGIS_910A* rock is close to pure silica, as indicated by the composition provided by the quantification model. The very high Si content of the target is also in agreement with spectral unmixing scores, a ‘calibration-free’ approach that derives semi-quantitative elemental abundances exclusively from spectral data (Schröder et al., 2023).

The relatively low MOC totals (73–87 wt.%, Table SOM1) may be due to the presence of one or a combination of the following non-quantified species: C, H, S, and Cl (but neither S nor Cl emission lines were detected, and the carbon signal is dominated by atmospheric signature). It is also possible that these low totals were affected by a degraded performance of the MOC algorithm on such extreme chemistry, since the calibration did not include many targets with SiO₂ >80 wt. % (see figure 11 in Anderson et al., 2022). Performance of the MOC on pure mineral phases are discussed in detail for other phases like olivine (Beyssac et al., 2023). Analysis of the hydrogen signal revealed that the hydrogen score is generally low in all targets (Fig. SOM3). This behavior is distinct from LIBS observations of opaline silica in Gale crater by ChemCam (Rapin et al., 2018; Gabriel et al., 2022), where the hydrogen signal was found to increase with SiO₂. This suggests a relatively low water content of the silica-rich material found in Jezero crater.

If present in sufficient amounts, SuperCam LIBS can also detect selected minor or trace elements (Li, Ni, Cu, Co, Ni, Ba, Rb, Sr, Cr, Mn, P, F; e.g. Wiens et al., 2021; Maurice et al., 2021).

4.3. IR-based mineralogy

The reflectance spectra of well-illuminated points (1–4) from *AEGIS_0910A* (Fig. 3) share an overall general blue slope and exhibit well-resolved absorptions at 1.9 µm (H₂O), 2.2 µm (Si-OH or Al-OH) and 1.4 µm (OH and H₂O). The chemistry derived from LIBS (SiO₂>70 wt.% and mean Al₂O₃< 2 wt.%) leads to the attribution of the 2.2 µm band to Si-OH instead of Al-OH. All such absorptions are present within spectra of terrestrial hydrated silica (Rice et al., 2013; Poitras et al., 2018). In addition, given the LIBS-derived chemistry, we assume that the target is dominated by hydrated silica and that these absorptions are related to this phase. Notably, the lack of sulfur signal in LIBS suggests that sulfates are at most, a minor phase in the target.

The reflectance spectra of *Elves_Chasm* also shows absorption bands near 1.4, 1.9 and 2.2 µm, but the exact position of these band differs from *AEGIS_0910A* (Fig. 3). In the case of *AEGIS_0910A*, the shape and position of the 1.9-µm band (centered at 1.944 µm) suggest that isolated H₂O molecules are a relatively minor component of the hydrated silica (Sun, 2017) since they typically have a maximum of absorption around 1.90 µm as observed in opal A (Fig. 3). The shape of the 2.2 µm band is more suggestive of a relatively mature form of hydrated silica where both hydrogen-bonded and isolated silanol (Si-OH) groups are present.

In the case of *Elves_Chasm*, the position of the 1.4 µm band (1.39 µm) and 2.2 µm band (2.205), as well as the relative intensity of the 2.2 and 1.9 µm band, are different from those measured for *AEGIS_910A*.

The use of spectral criteria can help decipher the forms of hydrated silica and their potential geological origins (Chauviré et al., 2017; Poitras et al., 2018; Sun et al., 2019; Pineau et al., 2023), and have been successfully applied to CRISM data (Pineau et al., 2020; Pan et al., 2021). These criteria (band depth, position and concavity) indicate that *AEGIS_0910A* has spectral properties close to terrestrial chalcodines (Fig. 3–B), while *Elves_Chasm* is similar to desiccated opals-A or CT. Calculation procedures for these spectral criteria are detailed in the Supplement Materials. (see also Figs. SOM 4 to 9).

The VISIR spectra obtained on *AEGIS_1311B* could not be exploited because of shadowing, but the three other targets from this location show very similar VISIR spectra (Fig. 3). While the LIBS-derived chemistry points toward very high SiO₂ compositions for these targets

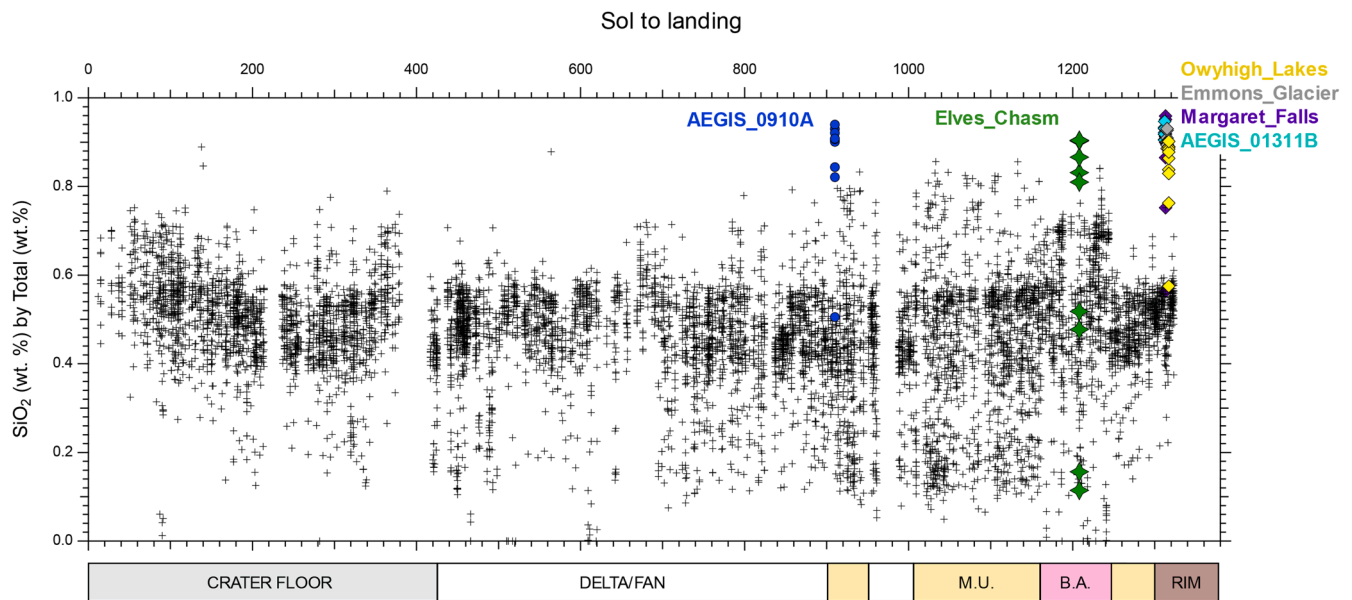


Fig. 2. SiO₂ abundance normalized to the total weight of oxides, for all SuperCam chemical analysis of rocks and soils since landing (targets <7 m). The colored symbols correspond to the 6 high-silica targets analyzed in this work. M.U.=Margin Unit. B.A.= Bright Angel.

encountered in the crater rim, the VISIR spectra do not show any evidence for Si-OH. This supports a mature form of silica in agreement with quartz detection by Raman in *Emmons_Glacier* (see next Section 4.4). Clear absorptions are still observed, that probably correspond to impurities within quartz. Absorption features at 2.31 and 2.39 μm are likely related to Mg-bearing clay minerals as found in the Margin Unit and some locations of the crater rim, while the absorption bands at 1.4, 1.9 and 2.1 μm may be related to the contribution from mono-hydrated Fesulfate (szomolnokite, Fig. 3).

4.4. Raman-based mineralogy

Only the *Emmons_Glacier* target was analyzed by Raman spectroscopy with a raster of ten points for LIBS and VISIR among which four points were analyzed. The four points yield very similar spectra, showing the same peaks and flat continuum background with same intensity, and absence of hydration features suggesting that the mineralogy is identical for these points. Averaging all these spectra gives the spectrum represented in Fig. 4 which unambiguously identifies quartz. All the peaks indicated by arrows in Fig. 4 are attributed to quartz as listed by Kingma and Hemley (1994), including lattice vibrations as well as most expected internal stretching and bending modes. Noticeably, no peak assignable to any other SiO₂ polymorph is observed in this spectrum (Kingma and Hemley, 1994), nor any feature including hydration assignable to opaline silica is detected (Ostrooumov et al. EJM 1999).

Looking at the spectral parameters after fitting using a pseudo-Voigt profile for the main peak shows that this peak has the expected Raman shift at $464.7 \pm 0.5 \text{ cm}^{-1}$ for quartz, and a full-width at half maximum (FWHM) of $\sim 15 \pm 1 \text{ cm}^{-1}$ in the average spectrum of Fig. 4. Analyzing each individual spectrum for the four points yields similar values to the average spectrum suggesting that the crystallinity is constant throughout the target. In Fig. 4A, the average spectrum of *Emmons_Glacier* shows striking similarity with the laboratory spectrum of a monocrystal of hydrothermal quartz with same peaks, absence of background and also similar FWHM: $\sim 15 \pm 1 \text{ cm}^{-1}$ versus $\sim 14 \pm 1 \text{ cm}^{-1}$ for *Emmons_Glacier* and the hydrothermal quartz, respectively. Fig. 4B depicts the Raman spectra obtained in the laboratory of the monocrystal of hydrothermal quartz compared to the spectra obtained with same acquisition parameters for the Fontainebleau sandstone and the Magadi chert. The main peaks are observed in all spectra but their

relative intensities are smaller in the sandstone and overall in the chert, while the background significantly increases from the hydrothermal quartz to the chert through the sandstone. Analysis of spectral parameters for the quartz main peak at 464 cm^{-1} shows that the peak FWHM slightly varies among the three targets with $\sim 16 \pm 1$, $\sim 14.6 \pm 1$, $\sim 14 \pm 1 \text{ cm}^{-1}$ in the hydrothermal quartz, the sandstone and the chert respectively.

5. Discussion

5.1. What type of silica / hydrated-silica?

To assess the formation process of the silica-dominated float rocks, a first step is to assess the type/crystallinity of silica material present.

In the case of target *Emmons_Glacier*, the Raman spectrum identifies unambiguously the presence of quartz (Fig. 4). Given the strong similarities in chemistry, texture and infrared spectra, it is likely that the other three float rocks from this location (*Owyhigh_Lakes*, *Margaret_Falls*, *AEGIS_1311B*) are also constituted by quartz.

In the case of *AEGIS_0910A* and *Elves_Chasm*, in the lack of Raman data, the identification of the type of silica material relies on IR data. The hydrated silica nomenclature is mostly based on the crystallographic arrangements, probed by X-ray diffraction, and therefore the SiO₄ tetrahedra network. This silica network can also be probed directly with mid-IR spectroscopy (such as what has been done in Gusev crater by the Miniature Thermal Emission Spectrometer - Ruff et al., 2011), but the wavelength range probed by SuperCam is only sensitive to harmonic and combination absorptions from H₂O and -OH groups. Still, several laboratory-based approaches have looked at how these modes vary as a function of the type of hydrated silica (see for instance: Rice et al., 2013; Sun, 2017; Chauviré, 2016). To further add to the complexity of hydrated silica near-IR spectroscopy, the various bands change as a function of environmental conditions (temperature, relative humidity) since part of the H₂O molecules can exchange more or less reversibly with the atmosphere (Poitras et al., 2018), or can crystallize under low-temperatures if grouped in sufficiently large domains (Sun, 2017; Chauviré et al., 2017).

The position and relative depths of absorption bands detected in *Elves_Chasm* are reminiscent of dehydrated opaline silica (Fig. 3A). This is confirmed by analyzing the position of the 1.4 and 2.2 μm bands,

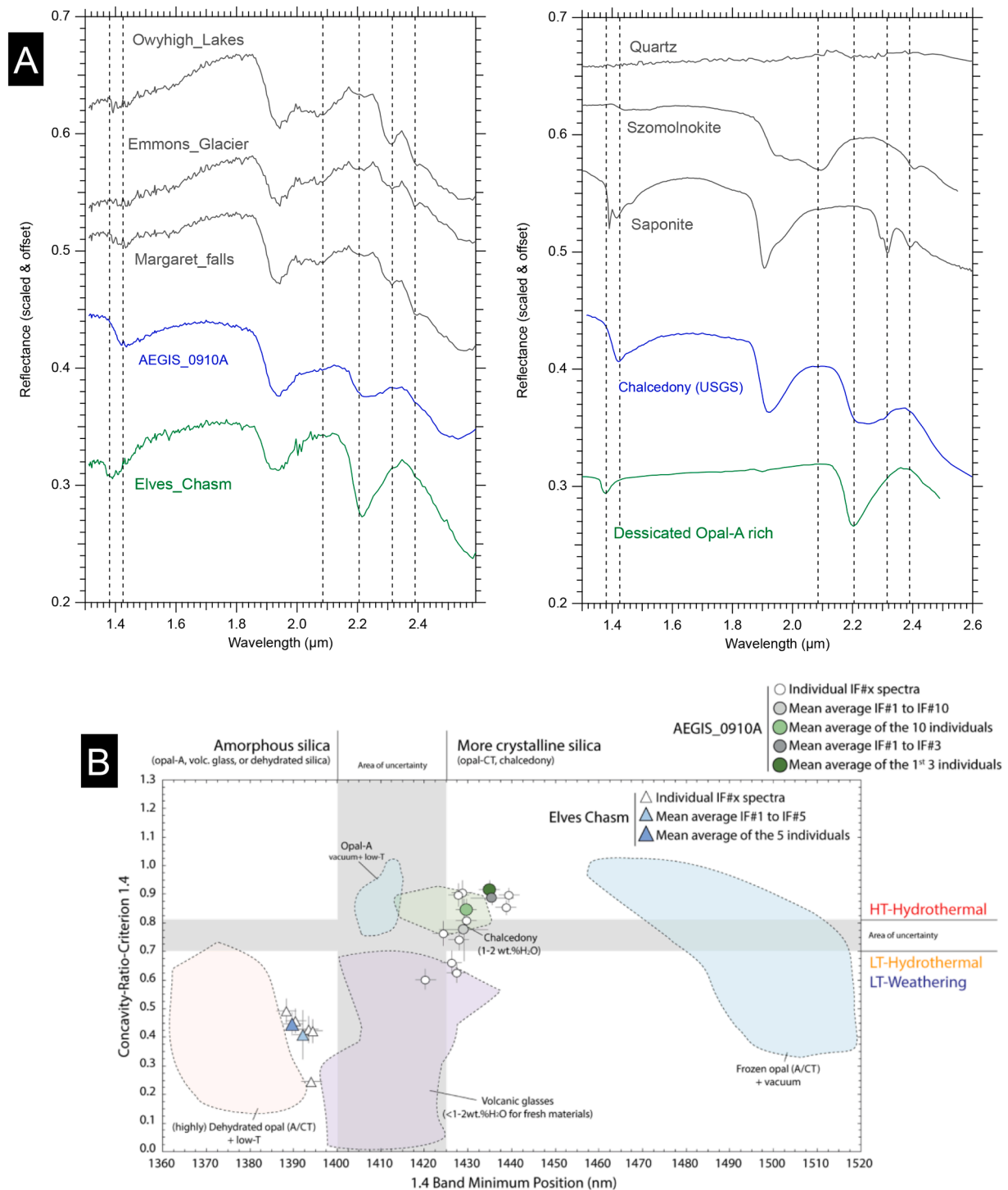


Fig. 3. A: Infrared reflectance spectra obtained on Mars by SuperCam on the silica-rich target compared to laboratory measurement on desiccated Opal-A (Sun et al., 2017), Opal-CT and chalcedony (USGS CU91-6A). The Quartz spectra is from USGS spectral library (GDS-31; Kokaly et al., 2017) and the Szomolnokite spectrum is from RELAB database (c1jb622a; https://sites.brown.edu/rehab/rehab-spectral-database). **B:** Example of classification diagram obtained using CRC1.4 (Concavity-Ratio-Criterion; Chauviré et al. 2017) that quantifies the shape of the 1.4 μm absorption as a function of the band minima position of the same absorption. Here, *AEGIS_0910A* tends to be close to the “chalcedony” field defined on terrestrial samples; which is also observed in Figs SOM4-9. Target *Elves Chasm* falls in the field of desiccated Opal-A / Opal-CT; Vertical error bars are twice the standard deviation from CRC calculation. Horizontal error bars are mean spectral resolution in the 1.4–1.6 μm range. For more information on nomenclature in the caption, please refer to Supplementary Materials.

which are in line with dehydrated Opal-A or Opal-CT (Fig. 3B, Figs. SOM4–9). While opaline silica may contain a significant fraction of weakly bonded water molecules inside its structure under terrestrial conditions, these may be lost upon exposure to the terrestrial atmosphere, leading to a decrease of the 1.9 μm and 2.26 μm band (Chauviré,

2016; Sun, 2017).

The position of absorption bands detected in *AEGIS_0910A* departs from what is typically observed for opal-A or opal-CT (i.e., the 1.9- μm band is at a longer wavelength in *AEGIS_0910A* and there is no clear 1.46- μm feature) and chalcedony is so far the closest spectral analog in

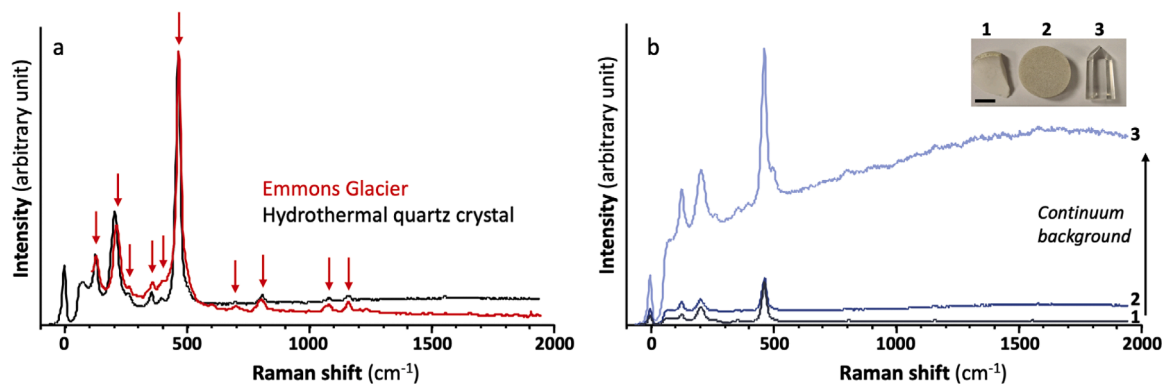


Fig. 4. a – Raman spectra of Emmons Glacier (red) and hydrothermal quartz crystal (black, depicted in b). No background correction, spectra are normalized to the maximum. Red arrows indicate the Raman peaks of quartz (Kingma and Hemley, 1994). b – Image (scale bar is 1 cm) and Raman spectra of the Magadi chert (1 – pale blue), the Fontainebleau sandstone (2 – dark blue) and the hydrothermal quartz crystal (3 - black). No background correction and no normalization. Note the increasing background continuum from the hydrothermal quartz to the Magadi chert.

terms of band position and shape. Chalcedony is a micro-crystalline type of silica, where the crystallites are fibrous and typically sub- μm in size. Chalcedony typically contains a few wt.% of “water” in the form of OH and H_2O (Graetsch et al., 1985; Chauviré et al., 2017) but is still usually referred to as a type of hydrated silica. The water in chalcedony can crystallize under low temperature, suggesting an occurrence as clusters of H_2O rather than isolated water molecules. Hydroxyl groups are present both as surface and internal silanols (Graetsch et al., 1985). On Earth, it can form in both sedimentary and volcanic environments, whether from direct precipitation from an aqueous fluid, as a response to evaporation, or a change of fluid temperature. Another frequent pathway to chalcedony is formation from opaline silica through an Ostwald ripening process (dissolution of smaller grains of opal and reprecipitation of larger grains of more crystalline silica, Heaney et al., 1994).

In summary, SuperCam has identified three types of high-silica material, of increasing maturity: opaline-silica, chalcedony, and quartz.

5.2. An hydrothermal origin of quartz-dominated float rocks

Quartz is found on Earth in igneous, metamorphic or sedimentary rocks. If the quartz were of igneous origin, we may expect to find it in close association with other silicates such as feldspar or micas, as well as with accessory minerals such as phosphates or Fe-Ti oxides. However, all the techniques (LIBS, Raman and VISIR) show that the targets are homogeneous (with the exception of superficial dust coatings) and that such phases are largely absent. Quartz may also be found in detrital sedimentary rocks like sandstones, but we do not see evidence for grains, cement, or other mineral phases that would support a sandstone hypothesis.

Quartz may also be encountered in cherts, rocks formed by the massive precipitation of silica. However, cherts are usually fine-grained and may produce a strong fluorescence-like background in remote Raman such as SuperCam (Fig 4b). Such background remains poorly understood but may result from a combination of effects, such as diffuse scattering at grains boundaries increasing the surficial versus volume interaction of the laser with grains in the target and/or the contribution of defects, including electronic defects within grains at grains boundaries (Clavé et al., 2024b). A contribution from organic fluorescence is also possible in the case of the chert. Note that such background is also observed in the sandstone although less intense compared to the chert (Fig. 4B). The *Emmons Glacier* spectrum shows a remarkably flat continuum background only comparable to the one observed in the spectrum of the transparent hydrothermal crystal. This suggests that the grain size is large in *Emmons Glacier*, at least significantly larger than the analytical footprint (~ 2.5 mm at that distance) and that the *crystallinity*

of quartz is very high in this target.

Therefore, our preferred hypothesis is that this well-crystalline quartz initially formed through slow precipitation from a warm aqueous fluid. On Earth quartz veins are commonly observed as fracture fills in crustal rocks and originate from the hydrothermal precipitation of silica. Such formation scenario would generate crystalline silica, and fairly coarse grain sizes and could explain the lack of fluorescence-like background. The clay-mineral identified by VISIR may have been entrained particles from the fluid flow in adjacent clay-rich lithologies, or may have directly precipitated from the fluid. The co-occurrence of possible szomolnokite (Fe-sulfate) could be explained by alteration of an Fe-sulfide precursor, that are commonly encountered within hydrothermal quartz veins.

Alternatively, silica can form in diagenetic settings at relatively low temperature (T). Here, the presence of phases of presumed higher T such as quartz suggest that near-surface diagenesis, as observed in Gale crater, is unlikely, and that a hydrothermal setting can more easily explain variations in the type of silica material encountered.

5.3. A suite of silica-dominated float rocks in Jezero crater and their shared origin

Hydrated-silica can be found on Earth in a variety of environments (volcanic, subsurface, subaerial/pedogenic, hydrothermal) where water interacts with silicates, producing dissolved SiO_2 into orthosilicic acid ($\text{Si}(\text{OH})_4$), which can then precipitate as a response to evaporation, to a change in pressure, temperature, or a modification of the fluid chemistry. This process can lead to the deposition of hydrated silica in volcanic environments, during terrestrial crustal weathering, or through direct precipitation in large bodies of water (i.e. cherts). In their article describing hydrated silica in Jezero, Tarnas et al. (2019) listed nine possible hypotheses for the origin of hydrated silica (supplementary Table S1 in Tarnas et al., 2019), that they grouped in three major formation processes: authigenic, volcanic, or detrital.

The composition derived from LIBS most likely rules out an origin as volcanic/igneous rocks for the quartz rocks but also for the other occurrences of high-silica targets. While the texture of *AEGIS 910A* may resemble that of a pumice (Fig. 1), the LIBS-derived composition of all 6 targets reveals a general depletion in mono-, di-, and tri-cations for most of the points (Table 1). Igneous processes may produce magmas with SiO_2 wt. % in the range of that determined for these rocks, but on Earth this silica enrichment is always associated with an enrichment in Al_2O_3 based on the elemental analysis of $>30,000$ evolved terrestrial rocks (dacites and rhyolites) from the GEOROC database (Fig. SOM10, Data were downloaded from the GEOROC database [https://georoc.eu] on July 8th 2024 using the following parameters: rock name=rhyolite,

rock_name=dacite). Rarely, rocks with $\text{SiO}_2 > 70$ wt. % and low Al_2O_3 (<5 wt.%) are described, but when they are, they tend to be either rich in TiO_2 (>10 wt. %) or FeO_T (ferro-rhyolite).

We can hypothesize that these three types of silica observed in Jezero are related to a single system and a single formation process. Given our preferred formation mechanism for quartz, precipitation from an aqueous fluid, we propose that the three types of silica material are hydrothermal in origin, and were formed under various conditions of precipitation, and possibly at various times. The texture and crystallinity of the quartz-dominated float rocks suggests direct precipitation of SiO_2 in a fluid, at moderate-T, and in a confined environment. On the other hand, the “popcorn” texture of *Elves Chasm*, may suggest precipitation under low-pressure (P), at the surface, as the texture is more akin to a surficial hydrothermal sinter deposit. We suggest that the three types of silica correspond to three distinct locations in a common hydrothermal system. In that model, the quartz-rich targets would have formed at some depth within the bedrock, while *Elves Chasm* may represent precipitates from a similar fluid but at the surface. The chalcedony target *AEGIS_0910A* would represent an intermediate level between the other opaline silica and the quartz. A schematic representation of this model inspired by Osinski et al. (2013) presented in Fig. 5. We should stress that this model involving a common origin is the simplest one. However, it is very possible that the three types of silica originate from multiple episodes of hydrothermalism or in multiple environments.

5.4. Source region of the silica-dominated float rocks

All silica-dominated rocks were found as float, making their source uncertain; they may have been transported from a yet-to-be sampled protolith by water or impact. The opaline silica (*Elves Chasm*) and the chalcedony float rock (*AEGIS_0910A*) were both found at the border of the Margin Unit of Jezero crater (Fig. 1). Grains of hydrated silica are present generally in the Margin Unit and in the crater floor units, but their mode of occurrence is clearly different from the silica-dominated float rocks we report here. In that case, hydrated silica is always found as pervasive in the bulk rock, as small grains (<0.5 μm), and in close textural association with the predominant carbonates and olivine phases. Hydrated silica grains in the Margin Unit and Séitah were probably formed by a carbonatation reaction of olivine (Clavé et al., 2024a).

If not related to the Margin Unit, these silica-dominated rocks could

have formed during the deposition of Jezero delta rocks or their diagenesis. These sediments were investigated extensively during a dedicated rover campaign on the delta top and delta front. Mafic minerals, Fe/Mg-carbonates, sulfates, and phyllosilicates were observed (Dehouck et al. 2024), but the rover did not encounter a pure hydrated silica-rich horizon, or discrete zones of Si diagenesis (e.g., opal alteration haloes). While circulation of alkaline fluids through sediments was found to produce hydrated silica fracture halos in Gale crater (Frydenvang et al. 2017), such diagenetic features were not observed in the sediments of the Jezero delta investigated by *Perseverance*. Also, the lack of observation of a silica-rich layer by the rover would tend to invalidate the hypothesis that the hydrated silica formed by direct deposition as sediment from the lake. It remains possible that such diagenetic or sedimentary silica exist, outside the area investigated by the rover, because of lateral facies variations. However, the observation of the quartz targets, which occurred above the expected lake level (Mangold et al., 2021), would appear to invalidate an origin related to lake activity.

Hydrated silica on Earth is often found as the alteration product of pre-existing rocks, commonly those of crustal felsic protoliths. Felsic rocks are depleted in Fe and Mg, rich in SiO_2 and their chemical leaching can lead to hydrated silica formation more easily than more mafic rocks. Such a process occurred for example in Australia where pedogenic and/or groundwater silcretes (silica crusts) are found and mined for gem-quality opals (Thiry and Milnes, 1991). These silcretes are built either by infiltrating meteoric waters that dissolved SiO_2 -rich rocks and soils (pedogenic silcrete) or by the interaction of the water table with clay minerals (groundwater silcrete) (Thiry and Milnes, 1991).

Felsic protoliths are absent in Jezero crater floor bedrock and delta sediments, but some were found during the first look at rocks from the crater rim. A suite of igneous rocks ranging from ultramafic (i.e. pyroxenite) to plagioclase-rich (i.e. anorthosite) was discovered by the rover in the crater rim. These evolved rocks may provide appropriate chemistries for silica-rich veins to form during hydrothermal circulation, provided that a heat source is available to initiate fluid flow. Interestingly, the quartz float rocks were found in the crater rim, close to a suspected fracture network. On Earth, impact cratering is known to generate hydrothermal systems within and around the crater, when the heat deposited by the cratering process is lost through water circulation (Osinski et al., 2013). In that case, hydrated silica and quartz are among

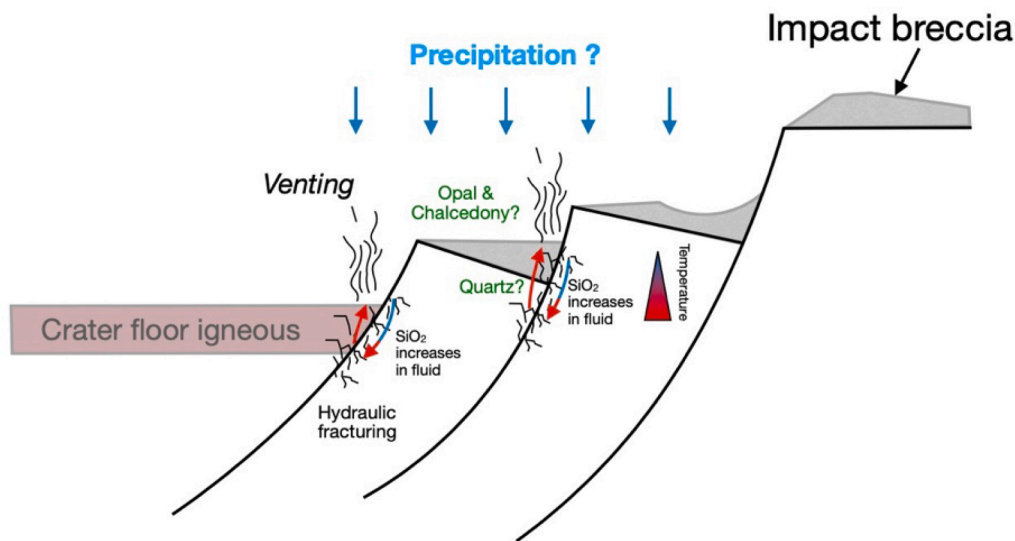


Fig. 5. Schematic of the proposed model to explain the precipitation of quartz, chalcedony and opal. Water infiltrates in the bedrock and SiO_2 concentration increases as the fluid percolates down. Warm fluids then ascend upward and silica can precipitate within the bedrock at some depth, where quartz may have formed. As the fluid reaches the surfaces, quick cooling and decompression leads to the precipitation of less crystalline forms, namely silica, opal and chalcedony. Inspired by Osinski et al. (2013).

the mineral phases that can be produced by such impact-induced hydrothermalism (Schwenzer and Kring, 2009; Osinski et al., 2013). In the case of terrestrial craters, deep faults are present on the crater rim/wall and at least in one well documented case, the Haughton crater, these faults were found to act as conduits for the development of hydrothermal vents (Osinski et al., 2005). Given the proximity of all silica-dominated targets with the Jezero crater wall, they could be related to a Noachian hydrothermal system, triggered by the Jezero crater forming event.

5.5. Astrobiological potential

The discovery of hydrated silica is promising for the search for organic traces of life on Mars (McMahon et al., 2018), since a hydrated silica matrix reduces the molecular degradation of fossil microorganisms over time, as demonstrated experimentally (Oehler, 1976; Alleon et al., 2016b). Even if Mars had never hosted life, the detection of hydrated silica along with crystalline silica may provide information on the ancient Martian organic system chemistry. The *Perseverance* rover's SHERLOC instrument was not able to analyze and hence assess the organic content of these samples due to engineering constraints, so we cannot speculate on the organic content of the float rocks. However, we can use the observed properties of the target to speculate on the organic preservation potential of similar materials at Jezero crater.

On Earth, hydrated opals inevitably evolved towards opal-CT, opal-C, and eventually quartz with time and burial diagenesis, classically via Ostwald ripening (Flörke et al., 1976; Oehler et al., 1976b), explaining the quasi-absence of opals older than a few tens of Ma (Rice et al., 2013). Yet, although organics have only a little affinity for monomeric silica, their presence may influence the fabric of silica sinters by affecting the crystallization rate of amorphous silica (Hinman, 1990; Yee et al., 2003; Konhauser et al., 2004). Since hydrogen bonds between amorphous silica and organics mainly occur with hydroxyl-bearing functional groups (Coradin and Livage, 2001; Konhauser et al., 2004), silica crystallization is likely to be retarded in the presence of hydroxyl-rich organic compounds. Such chemical interactions between organics and silica have been invoked to account for the detection of only partially recrystallized opals in ancient rocks (Moreau and Sharp, 2004). Thus, the presence of opaline silica could be related to the presence of organic compounds, making it a promising target to explore the organic chemistry that once existed on early Mars. While the rock described in this work was too small for drilling and collection, the *Perseverance* rover team will be looking for similar targets in the coming years.

Laboratory investigations of quartz would also be extremely interesting if any were to be included in future cached samples as part of the Mars Sample Return (MSR) program. Quartz is one of the best mineral hosts for fluid inclusions which may be used not only to further constrain the composition of the original fluid and conditions at which it precipitated, but also to investigate the possible presence of hydrocarbons and/or dissolved species.

CRedit authorship contribution statement

P. Beck: Writing – review & editing, Writing – original draft, Methodology, Investigation, Conceptualization. **O. Beyssac:** Writing – review & editing, Writing – original draft, Methodology, Investigation, Conceptualization. **E. Dehouck:** Writing – review & editing, Writing – original draft, Methodology, Investigation, Conceptualization. **S. Bernard:** Writing – review & editing, Writing – original draft, Methodology, Investigation, Conceptualization. **M. Pineau:** Writing – review & editing, Writing – original draft, Methodology, Investigation, Conceptualization. **L. Mandon:** Writing – review & editing, Writing – original draft, Methodology, Investigation, Conceptualization. **C. Royer:** Writing – review & editing, Writing – original draft, Methodology, Investigation, Conceptualization. **E. Clavé:** Writing – review & editing, Writing – original draft, Methodology, Investigation, Conceptualization. **S.**

Schröder: Writing – review & editing, Writing – original draft, Methodology, Investigation, Conceptualization. **O. Forni:** Writing – review & editing, Writing – original draft, Methodology, Investigation, Conceptualization. **R. Francis:** Writing – review & editing, Writing – original draft, Methodology, Investigation, Conceptualization. **N. Mangold:** Writing – review & editing, Writing – original draft, Methodology, Investigation, Conceptualization. **C.C. Bedford:** Writing – review & editing, Writing – original draft, Methodology, Investigation, Conceptualization. **A.P. Broz:** Writing – review & editing, Writing – original draft, Methodology, Investigation, Conceptualization. **E.A. Cloutis:** Writing – review & editing, Writing – original draft, Methodology. **J.R. Johnson:** Writing – review & editing, Writing – original draft, Methodology, Investigation, Conceptualization. **F. Poulet:** Writing – review & editing, Writing – original draft, Methodology, Investigation, Conceptualization. **T. Fouchet:** Writing – review & editing, Writing – original draft, Methodology, Investigation, Conceptualization. **C. Quantin-Nataf:** Writing – review & editing, Writing – original draft, Methodology, Investigation, Conceptualization. **C. Pilorget:** Writing – review & editing, Writing – original draft, Methodology, Investigation, Conceptualization. **W. Rapin:** Writing – review & editing, Writing – original draft, Methodology, Investigation, Conceptualization. **P.-Y. Meslin:** Writing – review & editing, Writing – original draft, Methodology. **T.S.J. Gabriel:** Writing – review & editing, Writing – original draft, Methodology, Investigation, Conceptualization. **G. Arana:** Writing – review & editing, Writing – original draft, Methodology, Investigation, Conceptualization. **J.M. Madariaga:** Writing – review & editing, Writing – original draft, Methodology, Investigation, Conceptualization. **A.J. Brown:** Writing – review & editing, Writing – original draft, Methodology, Investigation, Conceptualization. **S. Maurice:** Writing – review & editing, Writing – original draft, Methodology, Investigation, Conceptualization. **S.M. Clegg:** Writing – review & editing, Writing – original draft, Methodology, Investigation, Conceptualization. **O. Gasnault:** Writing – review & editing, Writing – original draft, Methodology, Investigation, Conceptualization. **A. Cousin:** Writing – review & editing, Writing – original draft, Methodology, Investigation, Conceptualization. **R.C. Wiens:** Writing – review & editing, Writing – original draft, Methodology, Investigation, Conceptualization.

Declaration of competing interest

The authors declare the following financial interests/personal relationships which may be considered as potential competing interests:

Beck reports financial support was provided by Centre National d'Etude Spatiale. Wiens reports financial support was provided by NASA. Francis reports financial support was provided by NASA. If there are other authors, they declare that they have no known competing financial interests or personal relationships that could have appeared to influence the work reported in this paper.

Acknowledgement

The authors are truly grateful for the SuperCam and Mars 2020 hardware operations teams for their investment in the mission. Funding from the Centre National d'Etude Spatiale (CNES) is acknowledged. This research was partly carried out at the Jet Propulsion Laboratory, California Institute of Technology, under a contract with the National Aeronautics and Space Administration (contract 80NM0018D0004). SC and RCW were supported by NASA (contract NNN13ZDA0180). The time-resolved Raman instrument at IMPMC (Paris) was funded by CNRS INP and Sorbonne Université grants. EAC acknowledges funding from the Canadian Space Agency (grant #EXPCO14) and the Natural Sciences and Engineering Research Council of Canada (grant #RGPIN-2023-03413). Any use of trade, firm, or product names is for descriptive purposes only and does not imply endorsement by the U.S. Government. JRJ was supported through JPL subcontract 1532432. This research

utilizes spectra acquired with the NASA RELAB facility at Brown University. We kindly acknowledge helpful comments from the three reviewers.

Supplementary materials

Supplementary material associated with this article can be found, in the online version, at [doi:10.1016/j.epsl.2025.119256](https://doi.org/10.1016/j.epsl.2025.119256).

Data availability

Data will be available on the PDS

References

- Alleon, J., Bernard, S., Le Guillou, C., Beyssac, O., Sugitani, K., Robert, F., 2018. Chemical nature of the 3.4 Ga strelley pool microfossils. *Geochem. Persp. Lett.* 37–42. <https://doi.org/10.7185/geochemlet.1817>.
- Alleon, J., Bernard, S., Le Guillou, C., Marin-Carbone, J., Pont, S., Beyssac, O., McKeegan, K.D., Robert, F., 2016a. Molecular preservation of 1.88 Ga gunflint organic microfossils as a function of temperature and mineralogy. *Nat. Commun.* 7 (1), 11977. <https://doi.org/10.1038/ncomms11977>.
- Alleon, J., Bernard, S., Le Guillou, C., Daval, D., Skouri-Panet, F., Pont, S., Delbes, L., Robert, F., 2016b. Early entombment within Silica minimizes the molecular degradation of microorganisms during advanced diagenesis. *Chem. Geol.* 437, 98–108. <https://doi.org/10.1016/j.chemgeo.2016.05.034>.
- Anderson, R.B., Forni, O., Cousin, A., Wiens, R.C., Clegg, S.M., Frydenvang, J., Gabriel, T. S.J., Ollila, A., Schröder, S., Beyssac, O., Gibbons, E., Vogt, D.S., Clavé, E., Manrique, J.-A., Legett, C., Pilleri, P., Newell, R.T., Sarrao, J., Maurice, S., Arana, G., Benzerara, K., Bernardi, P., Bernard, S., Bousquet, B., Brown, A.J., Alvarez-Llamas, C., Chide, B., Cloutis, E., Comellas, J., Connell, S., Dehouck, E., Delapp, D. M., Essunfeld, A., Fabre, C., Fouchet, T., García-Florentino, C., García-Gómez, L., Gasda, P., Gasnault, O., Hausrath, E.M., Lanza, N.L., Laserna, J., Lasue, J., Lopez, G., Madariaga, J.M., Mandon, L., Mangold, N., Meslin, P.-Y., Nelson, A.E., Newsom, H., Reyes-Newsom, A.L., Robinson, S., Rull, F., Sharma, S., Simon, J.L., Sobron, P., Fernandez, I.T., Udry, A., Venhaus, D., McLennan, S.M., Morris, R.V., Ehlmann, B., 2022. Post-landing major element quantification using SuperCam laser induced breakdown spectroscopy. *Spectrochim. Acta - Part B* 188, 106347. <https://doi.org/10.1016/j.sab.2021.106347>.
- Bandfield, J.L., Hamilton, V.E., Christensen, P.R., McSween, H.Y., 2004. Identification of quartzofeldspathic materials on Mars. *J. Geophys. Res. (Planets)* 109, E10009.
- Bandfield, J.L., 2008. High-silica deposits of an aqueous origin in Western Hellas Basin. *Mars. Geophys. Res. Lett.* 35, L12205.
- Bandfield, J.L., Amador, E.S., Thomas, N.H., 2013. Extensive hydrated silica materials in Western Hellas Basin. *Mars. Icarus* 226, 1489–1498.
- Beyssac, O., Forni, O., Cousin, A., Udry, A., Kah, L.C., Mandon, L., Clavé, O.E., Liu, Y., Poulet, F., Quantin Nataf, C., Gasnault, O., Johnson, J.R., Benzerara, K., Beck, P., Dehouck, E., Mangold, N., Alvarez-Llamas, C., Anderson, R.B., Arana, G., Barnes, R., Bernard, S., Bosak, T., Brown, A.J., Castro, K., Chide, B., Clegg, S.M., Cloutis, E., Fouchet, T., Gabriel, T., Gupta, S., Lacombe, G., Lasue, J., Le Mouéllic, S., Lopez-Reyes, G., Madariaga, J.M., McCubbin, F.M., McLennan, S.M., Manrique, J.A., Meslin, P.-Y., Montmessin, F., Núñez, J., Ollila, A.M., Ostwald, A., Pilleri, P., Pinet, P., Royer, C., Sharma, S.K., Schröder, S., Simon, J.L., Toplis, M.J., Veneranda, M., Willis, P.A., Maurice, S., Wiens, R.C., 2023. Petrological traverse of the Olivine Cumulate Séthah formation at Jezero Crater, Mars: a perspective from SuperCam onboard perseverance. *J. Geophys. Res. (Planets)* 128 e2022JE007638.
- Butterfield, N.J., 2003. Exceptional fossil preservation and the cambrian explosion. *Integr. Comp. Biol.* 43 (1), 166–177. <https://doi.org/10.1093/icb/43.1.166>.
- Carter, J., Riu, L., Poulet, F., Bibring, J.-P., Langevin, Y., Gondet, B., 2023. A Mars orbital catalog of aqueous alteration signatures (MOCAAS). *Icarus* 389, 115164.
- Chauviré, B., 2016. *Genèse De Silice Supergène Sur Terre Et Implications Sur Mars*. Université Nantes.
- Chauviré, B., Houadria, M., Donini, A., Berger, B.T., Rondeau, B., Kritsky, G., Lhuissier, P., 2020. Arthropod entombment in weathering-formed opal: new horizons for recording life in rocks. *Sci. Rep.* 10 (1), 10575. <https://doi.org/10.1038/s41598-020-67412-9>.
- Chauviré, B., Rondeau, B., Mangold, N., 2017. Near infrared signature of opal and chalcedony as a proxy for their structure and formation conditions. *Eur. J. Mineral.* 29, 409–421.
- Clavé, E., Beck, P., Dehouck, E., Forni, O., Schröder, S., Mangold, N., Royer, C., Mandon, L., Le Mouéllic, S., Quantin-Nataf, C., Bernard, S., Madariaga, J.A., Lopez-Reyes, G., Ollila, A., Johnson, J., Clegg, S., Cousin, A., Wiens, R.C., Maurice, S., 2024a. Diversity of carbonates in Jezero Crater, Mars, as seen with the SuperCam instrument. In: *LPI Contributions*, 3040. The Woodlands, Texas, p. 1829.
- Clavé, E., Benzerara, K., Meslin, P.-Y., Forni, O., Royer, C., Mandon, L., Beck, P., Quantin-Nataf, C., Beyssac, O., Cousin, A., Bousquet, B., Wiens, R.C., Maurice, S., Dehouck, E., Schröder, S., Gasnault, O., Mangold, N., Dromart, G., Bosak, T., Bernard, S., Udry, A., Anderson, R.B., Arana, G., Brown, A.J., Castro, K., Clegg, S.M., Cloutis, E., Fairén, A.G., Flannery, D.T., Gasda, P.J., Johnson, J.R., Lasue, J., Lopez-Reyes, G., Madariaga, J.M., Manrique, J.A., Le Mouéllic, S., Núñez, J.L., Ollila, A.M., Pilleri, P., Pilorget, C., Pinet, P., Poulet, F., Veneranda, M., Wolf, Z.U., 2023. The SuperCam team. Carbonate detection with SuperCam in igneous rocks on the floor of Jezero Crater. *Mars. JGR Planets* 128 (6), e2022JE007463. <https://doi.org/10.1029/2022JE007463>.
- Coradin, T., Livage, J., 2001. Effect of some amino acids and peptides on silicic acid polymerization. *Coll. Surf. B* 21 (4), 329–336. [https://doi.org/10.1016/S0927-7765\(01\)00143-6](https://doi.org/10.1016/S0927-7765(01)00143-6).
- Cousin, A., Sautter, V., Fabre, C., Dromart, G., Montagnac, G., Drouet, C., Meslin, P.-Y., Gasnault, O., Beyssac, O., Bernard, S., Cloutis, E., Forni, O., Beck, P., Fouchet, T., Johnson, J.R., Lasue, J., Ollila, A.M., De Parseval, P., Gouy, S., Caron, B., Madariaga, J.M., Arana, G., Madsen, M.B., Laserna, J., Moros, J., Manrique, J.A., Lopez-Reyes, G., Rull, F., Maurice, S., Wiens, R.C., 2022. SuperCam calibration targets on board the perseverance Rover: fabrication and quantitative characterization. *Spectrochim. Acta Part B* 188, 106341. <https://doi.org/10.1016/j.sab.2021.106341>.
- Dehouck, E., Forni, O., Quantin-Nataf, C., Beck, P., Mangold, N., Beyssac, O., Royer, C., Clavé, E., Johnson, J.R., Mandon, L., Poulet, F., Udry, A., Lopez-Reyes, G., Caravaca, G., Maurice, S., Wiens, R.C., Stack, K.M., Anderson, R.B., Bernard, S., Bosak, T., Broz, A.P., Castro, K., Clegg, S.M., Cousin, A., Dromart, G., Farley, K.A., Fouchet, T., Frydenvang, J., Gabriel, T.S.J., Gasda, P., Gibbons, E., Horgan, B.H.N., Hurowitz, J.A., Kalucha, H., Lasue, J., Le Mouéllic, S., Madariaga, J.M., Meslin, P.-Y., Nachon, M., Núñez, J.L., Pilleri, P., Pilorget, C., Rice, J.W., Russell, P.S., Schröder, S., Shuster, D.L., Siebach, K.L., Simon, J.L., Weiss, B.P., Williams, A.J., 2024. Chemostratigraphy and mineralogy of the Jezero Western Fan as seen by the SuperCam instrument: evidence for a complex aqueous history and variable alteration conditions. *LPI Contrib.*; Pasadena, California 3007, 3364.
- Farley, K.A., Williford, K.H., Stack, K.M., Bhartiya, R., Chen, A., de la Torre, M., Hand, K., Goreva, Y., Herd, C.D.K., Hueso, R., Liu, Y., Maki, J.N., Martinez, G., Moeller, R.C., Neelsen, A., Newman, C.E., Nunes, D., Ponce, A., Spanovich, N., Willis, P.A., Beegle, L.W., Bell, J.F., Brown, A.J., Hamran, S.-E., Hurowitz, J.A., Maurice, S., Paige, D.A., Rodriguez-Manfredi, J.A., Schulte, M., Wiens, R.C., 2020. Mars 2020 Mission overview. *Space Sci. Rev.* 216, 142.
- Fau, A., Beyssac, O., Gauthier, M., Meslin, P.-Y., Cousin, A., Benzerara, K., Bernard, S., Bouliard, J.C., Gasnault, O., Forni, O., Wiens, R.C., Morand, M., Rosier, P., Garino, Y., Pont, S., Maurice, S., 2019. Pulsed laser-induced heating of mineral phases: implications for laser-induced breakdown spectroscopy combined with raman spectroscopy. *Spectrochimica Acta - Part B* 160, 105687.
- Filiberto, J., Gross, J., Udry, A., Trella, J., Wittmann, A., Cannon, K.M., Penniston-Dorland, S., Ash, R., Hamilton, V.E., Meado, A.L., Carpenter, P., Jolliff, B., Ferré, E. C., 2018. Shergottite Northwest Africa 6963: a pyroxene-cumulate martian gabbro. *J. Geophys. Res. (Planets)* 123, 1823–1841.
- Flörke, O.W., Hollmann, R., von Rad, U., Rösch, H., 1976. Intergrowth and twinning in Opal-CT lepispheres. *Contrib. Mineral. Petrol.* 58, 235–242.
- Fouchet, T., Reess, J.-M., Montmessin, F., Hassen-Khodja, R., Nguyen-Tuong, N., Humeau, O., Jacquino, S., Lapauw, L., Parisot, J., Bonafous, M., Bernardi, P., Chapron, F., Jeanneau, A., Collin, C., Zegana, D., Nibert, P., Abbaki, S., Montaron, C., Blanchard, C., Arslanyan, V., Achelhi, O., Colon, C., Royer, C., Hamm, V., Beuzit, M., Poulet, F., Pilorget, C., Mandon, L., Forni, O., Cousin, A., Gasnault, O., Pilleri, P., Dubois, B., Quantin, C., Beck, P., Beyssac, O., Le Mouéllic, S., Johnson, J.R., McConnochie, T.H., Maurice, S., Wiens, R.C., 2022. The SuperCam infrared spectrometer for the perseverance rover of the Mars 2020 mission. *Icarus* 373, 114773.
- Francis, R., Estlin, T., Doran, G., Johnstone, S., Gaines, D., Verma, V., Burl, M., Frydenvang, J., Montañón, S., Wiens, R.C., Schaffer, S., Gasnault, O., DeFlores, L., Blaney, D., Bornstein, B., 2017. AEGIS autonomous targeting for ChemCam on Mars Science Laboratory: deployment and results of initial science team use. *Sci. Robot.* 2 (7), eaan4582. <https://doi.org/10.1126/scirobotics.aan4582>.
- Frydenvang, J., Gasda, P.J., Hurowitz, J.A., Grotzinger, J.P., Wiens, R.C., Newsom, H.E., Edgett, K.S., Watkins, J., Bridges, J.C., Maurice, S., Fisk, M.R., Johnson, J.R., Rapin, W., Stein, N.T., Clegg, S.M., Schwenzer, S.P., Bedford, C.C., Edwards, P., Mangold, N., Cousin, A., Anderson, R.B., Payré, V., Vaniman, D., Blake, D.F., Lanza, N.L., Gupta, S., Van Beek, J., Sautter, V., Meslin, P.-Y., Rice, M., Milliken, R., Gellert, R., Thompson, L., Clark, B.C., Sumner, D.Y., Fraeman, A.A., Kinch, K.M., Madsen, M.B., Mitrofanov, I.G., Jun, I., Calef, F., Vasavada, A.R., 2017. Diagenetic silica enrichment and late-stage groundwater activity in Gale Crater. *Mars. Geophys. Res. Lett.* 44, 4716–4724.
- Gabriel, T.S.J., Hardgrove, C., Achilles, C.N., Rampe, E.B., Rapin, W.N., Nowicki, S., Czarnecki, S., Thompson, L., Nikiforov, S., Litvak, M., Mitrofanov, I., Lisov, D., Frydenvang, J., Yen, A., Wiens, R.C., Treiman, A., McAdam, A., 2022. On an extensive late hydrologic event in Gale Crater as indicated by water-rich fracture halos. *J. Geophys. Res. (Planets)* 127, e2020JE006600.
- Graetsch, H., Florke, O.W., Mische, G., 1985. The nature of water un chalcedony and opal-C from Brazilian agate geodes. *Phys. Chem. Miner.* 300–306.
- Heaney, P.J., Prewitt, C.T., Gibbs, G.V., 1994. *Silica: Physical Behavior. Geochemistry and Materials Application*.
- Hinman, N.W., 1990. Chemical factors influencing the rates and sequences of silica phase transitions: effects of organic constituents. *Geochim. Cosmochim. Acta* 54, 1563–1574.
- Horgan, B.H.N., Anderson, R.B., Dromart, G., Amador, E.S., Rice, M.S., 2020. The mineral diversity of Jezero Crater: evidence for possible lacustrine carbonates on Mars. *Icarus* 339, 113526.
- Kingma, K.J., Hemley, R.J., April 1, 1994. Raman spectroscopic study of microcrystalline silica. *Am. Mineralog.* 269–273.
- Kokaly, R.F., Clark, R.N., Swayze, G.A., Livo, K.E., Hoefen, T.M., Pearson, N.C., Wise, R. A., Benzel, W.M., Lowers, H.A., Driscoll, R.L., Klein, A.J. (2017) USGS Spectral Library version 7 Dara: US.S. Geological Survey data releases <https://doi.org/10.5066/F7RR1WJD>.

- Konhauser, K.O., Jones, B., Phoenix, V.R., Ferris, G., Renaut, R.W., 2004. The microbial role in hot spring silicification. *AMBIO* 33 (8), 552–558. <https://doi.org/10.1579/0044-7447-33.8.552>.
- Liu, Y., Wu, X., Zhao, Y.-Y.S., Pan, L., Wang, C., Liu, J., Zhao, Z., Zhou, X., Zhang, C., Wu, Y., Wan, W., Zou, Y., 2022. Zhurong reveals recent aqueous activities in Utopia Planitia. *Mars. Sci. Adv.* 8 (19), eabn8555. <https://doi.org/10.1126/sciadv.abn8555>.
- Mangold, N., Gupta, S., Gasnault, O., Dromart, G., Tarnas, J.D., Sholes, S.F., Horgan, B., Quantin-Nataf, C., Brown, A.J., Le Mouélic, S., Yngst, R.A., Bell, J.F., Beyssac, O., Bosak, T., Calef, F., Ehlmann, B.L., Farley, K.A., Grotzinger, J.P., Hickman-Lewis, K., Holm-Alwmark, S., Kah, L.C., Martínez-Frías, J., McLennan, S.M., Maurice, S., Nuñez, J.I., Ollila, A.M., Pilleri, P., Rice, J.W., Rice, M., Simon, J.I., Shuster, D.L., Stack, K.M., Sun, V.Z., Treiman, A.H., Weiss, B.P., Wiens, R.C., Williams, A.J., Williams, N.R., Williford, K.H., 2021. Perseverance rover reveals an ancient Delta-Lake system and flood deposits at Jezero Crater. *Mars. Science* 374, 711–717.
- Maurice, S., Wiens, R.C., Bernardi, P., Cais, P., Robinson, S., Nelson, T., Gasnault, O., Reess, J.-M., Deleuze, M., Rull, F., Manrique, J.-A., Abbaki, S., Anderson, R.B., André, Y., Angel, S.M., Arana, G., Battault, T., Beck, P., Benzerara, K., Bernard, S., Berthias, J.-P., Beyssac, O., Bonafoux, M., Bousquet, B., Boutillier, M., Cadu, A., Castro, K., Chapron, F., Chide, B., Clark, K., Clavé, E., Clegg, S., Cloutis, E., Collin, C., Córdoba, E.C., Cousin, A., Dameury, J.-C., D'Anna, W., Daydou, Y., Debus, A., Deflores, L., Dehouck, E., Delapp, D., De Los Santos, G., Donny, C., Doressoundiram, A., Dromart, G., Dubois, B., Dufour, A., Dupieux, M., Egan, M., Ervin, J., Fabre, C., Fau, A., Fischer, W., Forni, O., Fouchet, T., Frydenvang, J., Gauffre, S., Gauthier, M., Gharakanian, V., Gilard, O., Gontijo, I., Gonzalez, R., Granena, D., Grotzinger, J., Hassen-Khodja, R., Heim, M., Hello, Y., Hervet, G., Humeau, O., Jacob, X., Jacquino, S., Johnson, J.R., Kouach, D., Lacombe, G., Lanza, N., Lapauw, L., Laserna, J., Lasue, J., Le Deit, L., Le Mouélic, S., Le Comte, E., Lee, Q.-M., Leggett, C., Leveille, R., Lewin, E., Leyrat, C., Lopez-Reyes, G., Lorenz, R., Lucero, B., Madariaga, J.M., Madsen, S., Madsen, M., Mangold, N., Manni, F., Mariscal, J.-F., Martínez-Frías, J., Mathieu, K., Mathon, R., McCabe, K.P., McConnochie, T., McLennan, S.M., Mekki, J., Melikechi, N., Meslin, P.-Y., Micheau, Y., Michel, Y., Michel, J.M., Mimoun, D., Misra, A., Montagnac, G., Montaron, C., Montmessin, F., Moros, J., Mousset, V., Morizet, Y., Murdoch, N., Newell, R.T., Newsom, H., Nguyen Tuong, N., Ollila, A.M., Orttog, G., Oudda, L., Pares, L., Parisot, J., Parot, Y., Pérez, R., Pheav, D., Picot, L., Pilleri, P., Pilorget, C., Pinet, P., Pont, G., Poulet, F., Quantin-Nataf, C., Quertier, B., Rambaud, D., Rapin, W., Romano, P., Roucayrol, L., Royer, C., Ruellan, M., Sandoval, B.F., Sautter, V., Schoppers, M.J., Schröder, S., Seran, H.-C., Sharma, S.K., Sobron, P., Sodki, M., Sournac, A., Sridhar, V., Standardovsky, D., Storms, S., Striebig, N., Tatat, M., Toplis, M., Torre-Pdeiz, L., Toulemont, N., Velasco, C., Veneranda, M., Venhaus, D., Virmontois, C., Viso, M., Willis, P., Wong, K.W., 2021. The SuperCam instrument Suite on the Mars 2020 Rover: science objectives and mast-unit description. *Space Sci. Rev.* 217, 47.
- McMahon, S., Bosak, T., Grotzinger, J.P., Milliken, R.E., Summons, R.E., Daye, M., Newman, S.A., Fraeman, A., Williford, K.H., Briggs, D.E.G., 2018. A field guide to finding fossils on Mars. *JGR Planets* 123 (5), 1012–1040. <https://doi.org/10.1029/2017JE005478>.
- Milliken, R.E., Swayze, G.A., Arvidson, R.E., Bishop, J.L., Clark, R.N., Ehlmann, B.L., Green, R.O., Grotzinger, J.P., Morris, R.V., Murchie, S.L., Mustard, J.F., Weitz, C., 2008. Silica in young deposits on Mars. *Geology*, 36, 847–850.
- Moreau, J.W., Sharp, T.G., 2004. A transmission electron microscopy study of silica and kerogen biosignatures in 1.9 Ga gunflint microfossils. *Astrobiology*, 4 (2), 196–210. <https://doi.org/10.1089/153110704323175142>.
- Morris, R.V., Ruff, S.W., Gellert, R., Ming, D.W., Arvidson, R.E., Clark, B.C., Golden, D.C., Siebach, K., Klingelhöfer, G., Schröder, C., Fleischer, I., Yen, A.S., Squyres, S.W., 2010. Identification of carbonate-rich outcrops on Mars by the Spirit Rover. *Science* (1979) 329 (5990), 421–424. <https://doi.org/10.1126/science.1189667>.
- Morris, R.V., Vaniman, D.T., Blake, D.F., Gellert, R., Chipera, S.J., Rampe, E.B., Ming, D.W., Morrison, S.M., Downs, R.T., Treiman, A.H., Yen, A.S., Grotzinger, J.P., Achilles, C.N., Bristow, T.F., Crisp, J.A., Des Marais, D.J., Farmer, J.D., Fendrich, K.V., Frydenvang, J., Graff, T.G., Morookian, J.-M., Stolper, E.M., Schwenzer, S.P., 2016. Silicic volcanism on Mars evidenced by tridymite in high-SiO₂ sedimentary rock at Gale Crater. *Proc. Nation. Acad. Sci.* 113, 7071–7076.
- Oehler, J.H., 1976. Experimental studies in precambrian paleontology: structural and chemical changes in blue-green algae during simulated fossilization in synthetic chert. *Geol. Soc. Am. Bull.* 87, 117.
- Osinski, G.R., Tornabene, L.L., Banerjee, N.R., Cockell, C.S., Flemming, R., Izawa, M.R.M., McCutcheon, J., Parnell, J., Preston, L.J., Pickersgill, A.E., Pontefract, A., Sapers, H.M., Southam, G., 2013. Impact-generated hydrothermal systems on Earth and Mars. *Icarus* 224, 347–363.
- Ostrooumov, M., Fritsch, E., Lasnier, B., Lefrant, S., September 30, 1999. Spectres Raman Des Opales: aspect diagnostique et aide à La Classification. *Eur. J. Mineral.* 899–908.
- Pan, L., Ehlmann, B.L., 2014. Phyllosilicate and hydrated silica detections in the knobby terrains of Acidalia Planitia, Northern Plains, Mars. *Geophys. Res. Lett.* 41, 1890–1898.
- Pan, L., Carter, J., Quantin-Nataf, C., Pineau, M., Chauviré, B., Mangold, N., Le Deit, L., Rondeau, B., Chevrier, V., 2021. Voluminous silica precipitated from martian waters during late-stage aqueous alteration. *Planet. Sci. J.* 2, 65.
- Pineau, M., Le Deit, L., Chauviré, B., Carter, J., Rondeau, B., Mangold, N., 2020. Toward the geological significance of hydrated silica detected by near infrared spectroscopy on Mars based on terrestrial reference samples. *Icarus* 347, 113706.
- Pineau, M., Chauviré, B., Rondeau, B., 2023. Near-infrared signature of hydrothermal opal: a case study of Icelandic silica sinters. *Eur. J. Mineral.* 35 (6), 949–967. <https://doi.org/10.5194/ejm-35-949-2023>.
- Rampe, E.B., Laporte, M.G.A., Bristow, T.F., Arvidson, R.E., Morris, R.V., Achilles, C.N., Weitz, C., Blake, D.F., Ming, D.W., Morrison, S.M., Vaniman, D.T., Chipera, S.J., Downs, R.T., Grotzinger, J.P., Hazen, R.M., Peretyazhko, T.S., Sutter, B., Tu, V., Yen, A.S., Horgan, B., Castle, N., Craig, P.I., Des Marais, D.J., Farmer, J., Gellert, R., McAdam, A.C., Morookian, J.M., Sarrazin, P.C., Treiman, A.H., 2018. Sand mineralogy within the Bagnold Dunes, Gale Crater, as observed In situ and from orbit. *Geophys. Res. Lett.* 45, 9488–9497.
- Rapin, W., Chauviré, B., Gabriel, T.S.J., McAdam, A.C., Ehlmann, B.L., Hardgrove, C., Meslin, P.-Y., Rondeau, B., Dehouck, E., Franz, H.B., Mangold, N., Chipera, S.J., Wiens, R.C., Frydenvang, J., Schröder, S., 2018. In situ analysis of opal in Gale Crater. *Mars. J. Geophys. Res. (Planets)* 123, 1955–1972.
- Rice, M.S., Cloutis, E.A., Bell, J.F., Bish, D.L., Horgan, B.H., Mertzman, S.A., Craig, M.A., Renaut, R.W., Gautason, B., Mountain, B., 2013. Reflectance spectra diversity of silica-rich materials: sensitivity to environment and implications for detections on Mars. *Icarus* 223, 499–533.
- Royer, C., Fouchet, T., Mandon, L., Montmessin, F., Poulet, F., Forni, O., Johnson, J.R., Leggett, C., Le Mouélic, S., Gasnault, O., Quantin-Nataf, C., Beck, P., Dehouck, E., Clavé, E., Ollila, A.M., Pilorget, C., Bernardi, P., Reess, J.-M., Pilleri, P., Brown, A., Newell, R.T., Cloutis, E., Maurice, S., Wiens, R.C., 2023. The SuperCam team. Reflectance of Jezero Crater floor: 1. Data processing and calibration of the infrared spectrometer (IRS) on SuperCam. *JGR Planets* 128 (1), e2022JE007481. <https://doi.org/10.1029/2022JE007481>.
- Ruff, S.W., Farmer, J.D., Calvin, W.M., Herkenhoff, K.E., Johnson, J.R., Morris, R.V., Rice, M.S., Arvidson, R.E., Bell, J.F., Christensen, P.R., Squyres, S.W., 2011. Characteristics, distribution, origin, and significance of Opaline Silica observed by the Spirit rover in Gusev Crater. *Mars. J. Geophys. Res.* 116, E00F23. <https://doi.org/10.1029/2010JE003767>.
- Schröder, S., Rammelkamp, K., Hansen, P.B., Seel, F., Cousin, A., Forni, O., Gasnault, O., Meslin, P.-Y., Pilleri, P., Rapin, W., Clavé, E., Dehouck, E., Beyssac, O., Beck, P., Maurice, S., Wiens, R.C., Hübers, H.-W., 2023. Semiquantitative analysis of ChemCam and SuperCam LIBS data with spectral unmixing. In: 54th Lunar and Planetary Science Conference, 2806. The Woodlands, Texas. Volp 2014.
- Schwenzer, S.P., Kring, D.A., 2009. Impact-generated hydrothermal systems capable of forming phyllosilicates on noachian Mars. *Geology*, 37, 1091–1094.
- Skok, J.R., Mustard, J.F., Ehlmann, B.L., Milliken, R.E., Murchie, S.L., 2010. Silica deposits in the Nili Patera Caldera on the Syrtis major Volcanic Complex on Mars. *Nat. Geosci.* 3, 838–841.
- Smith, M.R., Bandfield, J.L., Cloutis, E.A., Rice, M.S., 2013. Hydrated silica on Mars: combined analysis with near-infrared and thermal-infrared spectroscopy. *Icarus* 223, 633–648.
- Smith, R.J., McLennan, S.M., Achilles, C.N., Dehouck, E., Horgan, B.H.N., Mangold, N., Rampe, E.B., Salvatore, M., Siebach, K.L., Sun, V.X Ray, 2021. Amorphous components in sedimentary rocks of Gale Crater, Mars: evidence for ancient formation and long lived aqueous activity. *J. Geophys. Res. (Planets)* 126, e06782.
- Squyres, S.W., Arvidson, R.E., Ruff, S., Gellert, R., Morris, R.V., Ming, D.W., Crumpler, L., Farmer, J.D., Des Marais, D.J., Yen, A., McLennan, S.M., Calvin, W., Bell, J.F., Clark, B.C., Wang, A., McCoy, T.J., Schmidt, M.E., de Souza, P.A., 2008. Detection of silica-rich deposits on Mars. *Science* (1979) 320, 1063.
- Sun, V., 2017. Clays and Opals on Mars: Implications for Water-Rock Interactions Through Time. Brown University.
- Sun, V.Z., Milliken, R.E., 2018. Distinct geologic settings of opal-A and more crystalline hydrated silica on Mars. *Geophys. Res. Lett.* 45, 228, 10.1029/2017-10.
- Tarnas, J.D., Mustard, J.F., Lin, H., Goudge, T.A., Amador, E.S., Bramble, M.S., Kremer, C.H., Zhang, X., Itoh, Y., Parente, M., 2019. Orbital identification of hydrated silica in Jezero Crater. *Mars. Geophys. Res. Lett.* 46, 782, 12, 771–12.
- team, the S. S. Clavé, E., Beyssac, O., Bernard, S., Royer, C., Lopez-Reyes, G., Schröder, S., Rammelkamp, K., Forni, O., Fau, A., Cousin, A., Manrique, J.A., Ollila, A., Madariaga, J.M., Aramendia, J., Sharma, S.K., Fornaro, T., Maurice, S., Wiens, R.C., Acosta-Maeda, T., Agard, C., Alberquilla, F., Alvarez Llamas, C., Anderson, R., Applin, D., Aramendia, J., Arana, G., Beal, R., Beck, P., Bedford, C., Benzerara, K., Bernard, S., Bernardi, P., Bertrand, T., Beyssac, O., Bloch, T., Bonnet, J.-Y., Bousquet, B., Boustelstane, A., Bouyssou Mann, M., Brand, M., Cais, P., Caravaca, G., Castro Ortiz De Pinedo, K., Cazalla, C., Charpentier, A., Chide, B., Clavé, E., Clegg, S., Cloutis, E., Coloma, L., Comellas, J., Connell, S., Cousin, A., DeFlores, L., Dehouck, E., Delapp, D., Delgado Perez, T., Deron, J., Donny, C., Doressoundiram, A., Dromart, G., Essunfeld, A., Fabre, C., Fau, A., Fischer, W., Follic, H., Forni, O., Fouchet, T., Francis, R., Frydenvang, J., Gabriel, T., Gallegos, Z., García-Florentino, C., Gasda, P., Gasnault, O., Gibbons, E., Gillier, M., Gomez, L., Gonzalez, S., Grotzinger, J., Huidobro, J., Jacob, X., Johnson, J., Kalucha, H., Kelly, E., Knutsen, E., Lacombe, G., Lamarque, F., Lanza, N., Larmat, C., Laserna, J., Lasue, J., Le Deit, L., Le Mouélic, S., Leggett, C., Leveille, R., Lewin, E., Little, C., Loche, M., Lopez Reyes, G., Lorenz, R., Lorigny, E., Madariaga, J.M., Madsen, M., Mandon, L., Manelski, H., Mangold, N., Martinez, J.M., Martin, N., Martinez Frías, J., Maurice, S., McConnochie, T., McLennan, S., Melikechi, N., Meslin, P.-Y., Meunier, F., Mimoun, D., Montagnac, G., Montmessin, F., Moros, J., Mousset, V., Murdoch, N., Nelson, T., Newell, R., Nicolas, C., Newsom, H., O'Shea, C., Ollila, A., Pantalacci, P., Parmentier, J., Peret, L., Perrachon, P., Pilleri, P., Pilorget, C., Pinet, P., Poblacion, I., Poulet, F., Quantin Nataf, C., Rapin, W., Reyes, I., Rigaud, L., Robinson, S., Rochas, L., Root, M., Ropert, E., Rouverand, L., Royer, C., Rull Perez, F., Said, D., Sans-Jofre, P., Schroeder, S., Seel, F., Sharma, S., Sheridan, A., Sobron Sanchez, P., Stcherbinine, A., Stott, A., Toplis, M., Turenne, N., Veneranda, M., Venhaus, D., Wiens, R., Wolf, U., Zastrow, A., 2024b. Radiation-induced alteration of apatite on the surface of Mars: first in situ observations with SuperCam raman onboard perseverance. *Sci. Rep.* 14, 11284.
- Thiry, M., Milnes, A.R., 1991. Pedogenic and groundwater silicreets at Stuart Creek Opal Field South Australia. *J. Sediment. Petrol.* 111–127.
- Udry, A., Ostwald, A., Sautter, V., Cousin, A., Beyssac, O., Forni, O., Dromart, G., Benzerara, K., Nachon, M., Horgan, B., Mandon, L., Clavé, E., Dehouck, E., Gibbons,

- E.; Alwmark, S.; Ravanis, E.; Wiens, R.C.; Legett, C.; Anderson, R.; Pilleri, P.; Mangold, N.; Schmidt, M.; Liu, Y.; Núñez, J.I.; Castro, K.; Madariaga, J.M.; Kizovski, T.; Beck, P.; Bernard, S.; Bosak, T.; Brown, A.; Clegg, S.; Cloutis, E.; Cohen, B.; Connell, S.; Crumpler, L.; Debaille, V.; Flannery, D.; Fouchet, T.; Gabriel, T.S.J.; Gasnault, O.; Herd, C.D.K.; Johnson, J.; Manrique, J.A.; Maurice, S.; McCubbin, F.M.; McLennan, S.; Ollila, A.; Pinet, P.; Quantin-Nataf, C.; Royer, C.; Sharma, S.; Simon, J. I.; Steele, A.; Tosca, N.; Treiman, A.A. Mars 2020 Perseverance SuperCam perspective on the igneous nature of the Máaz Formation at Jezero Crater and link with Séítah, Mars. *J. Geophys. Res. (Planets)*, 2023, 128, e2022JE007440.
- Walsh, M.M., Lowe, D.R., 1985. Filamentous microfossils from the 3,500-myr-old Onverwacht Group, Barberton Mountain Land, South Africa. *Nature* 314 (6011), 530–532. <https://doi.org/10.1038/314530a0>.
- Wiens, R.C., Maurice, S., Robinson, S.H., Nelson, A.E., Cais, P., Bernardi, P., Newell, R.T., Clegg, S., Sharma, S.K., Storms, S., Deming, J., Beckman, D., Ollila, A.M., Gasnault, O., Anderson, R.B., André, Y., Michael Angel, S., Arana, G., Auden, E., Beck, P., Becker, J., Benzerara, K., Bernard, S., Beysac, O., Borges, L., Bousquet, B., Boyd, K., Caffrey, M., Carlson, J., Castro, K., Celis, J., Chide, B., Clark, K., Cloutis, E., Córdoba, E.C., Cousin, A., Dale, M., Deflores, L., Delapp, D., Deleuze, M., Dirmyer, M., Donny, C., Dromart, G., George Duran, M., Egan, M., Ervin, J., Fabre, C., Fau, A., Fischer, W., Forni, O., Fouchet, T., Fresquez, R., Frydenvang, J., Gasway, D., Gontijo, I., Grotzinger, J., Jacob, X., Jacquinos, S., Johnson, J.R., Klisiewicz, R.A., Lake, J., Lanza, N., Laserna, J., Lasue, J., Le Mouélic, S., Legett, C., Leveille, R., Lewin, E., Lopez-Reyes, G., Lorenz, R., Lorigny, E., Love, S.P., Lucero, B., Madariaga, J.M., Madsen, M., Madsen, S., Mangold, N., Manrique, J.A., Martinez, J. P., Martinez-Frias, J., McCabe, K.P., McConnochie, T.H., McGlown, J.M., McLennan, S.M., Melikechi, N., Meslin, P.-Y., Michel, J.M., Mimoun, D., Misra, A., Montagnac, G., Montmessin, F., Mousset, V., Murdoch, N., Newsom, H., Ott, L.A., Ousnamer, Z.R., Pares, L., Parot, Y., Pawluczyk, R., Glen Peterson, C., Pilleri, P., Pinet, P., Pont, G., Poulet, F., Provost, C., Quertier, B., Quinn, H., Rapin, W., Reess, J.-M., Regan, A.H., Reyes-Nowell, A.L., Romano, P.J., Royer, C., Rull, F., Sandoval, B., Sarrao, J.H., Sautter, V., Schoppers, M.J., Schröder, S., Seitz, D., Shepherd, T., Sobron, P., Dubois, B., Sridhar, V., Toplis, M.J., Torre-Fdez, I., Trettel, I.A., Underwood, M., Valdez, A., Valdez, J., Venhaus, D., Willis, P., 2021. The SuperCam instrument suite on the NASA Mars 2020 Rover: body unit and combined system tests. *Space Sci. Rev.* 217, 4.
- Yee, N., Phoenix, V.R., Konhauser, K.O., Benning, L.G., Ferris, F.G., 2003. The effect of cyanobacteria on silica precipitation at neutral pH: implications for bacterial silicification in geothermal hot springs. *Chem. Geol.* 199, 83–90.
- Yen, A.S., Ming, D.W., Vaniman, D.T., Gellert, R., Blake, D.F., Morris, R.V., Morrison, S. M., Bristow, T.F., Chipera, S.J., Edgett, K.S., Treiman, A.H., Clark, B.C., Downs, R.T., Farmer, J.D., Grotzinger, J.P., Rampe, E.B., Schmidt, M.E., Sutter, B., Thompson, L. M., 2017. Multiple stages of aqueous alteration along fractures in Mudstone and Sandstone strata in Gale Crater, Mars. *Earth Planet. Sci. Lett.* 471, 186–198. <https://doi.org/10.1016/j.epsl.2017.04.033>.